Applied Materials Today

Dual-Ionic Hydrogels with Ultralong Anti-dehydration Lifespan and Superior Anti-icing Performance

--Manuscript Draft--

Manuscript Number:	APMT-D-21-02463R1
Article Type:	Research Paper
Keywords:	dual-ionic hydrogel; anti-dehydration; Anti-icing; anti-frost; Long lifespan
Corresponding Author:	Tong Li Ningbo Institute of Materials Technology and Engineering CAS: Ningbo Institute of Industrial Technology Chinese Academy of Sciences Ningbo, 33 CHINA
First Author:	Tong Li
Order of Authors:	Tong Li
	Ke Xu
	Lianxin Shi
	Jianyang Wu
	Jianying He
	Zhiliang Zhang
Abstract:	Water-rich hydrogels find a wide range of promising applications due to their combined solid/liquid-like properties. However, hydrogels often exhibit a short lifespan and suffer from functional failure due to water depletion via rapid evaporation and icing/freezing under low temperatures. To tackle these challenges, here we developed a Ca 2+ and hydrophilic bonded -SO 3 - group-based dual-ionic hydrogel (DIH) which possesses an ultralong anti-dehydration lifespan and outstanding anti-icing properties. The as-developed DIH can keep wet and flexible as its initial state for longer than 8 months in practical room environment (15-35 o C, relative humidity of 30-90%), and show low ice adhesion of 2.3 kPa and durably frost-free property at -10.0 ℃ as well as anti-freezing property down to -49.0 ℃. According to the molecular dynamic simulations and experimental results, the superior anti-dehydration performances are due to the low-diffusion and high absorption capacity and self-replenishment of water via the dual-ionic strategy; the sufficient anti-icing Ca 2+ result in the extremely low melting point and anti-icing properties of the DIH. This design sheds new light on developing next-generation durable hydrogels with applications in soft materials and functional surfaces under harsh conditions of both low humidity and low temperatures.
Suggested Reviewers:	Jianjun Wang Key Laboratory of Green Printing Institute of Chemistry Chinese Academy of Sciences, Beijing 100190, China wangj220@iccas.ac.cn Prof. Jianjun Wang is a leading expert in anti-icing hydrogel.
	Zhigang Su School of Engineering and Applied Sciences and Kavli Insitute for Bionano Science and Technology, Harvard University suo@seas.harvard.edu He is an leading expert in the anti-freezing hydrogel
	Qinghua Zhang Zhejiang University qhzhang@zju.edu.cn Prof. Zhang is an expert in surface science and coatings.
Opposed Reviewers:	
Response to Reviewers:	

- The DIH design is proposed with hygroscopic free ions and hydrophilic bonded groups.
- The DIH possesses an ultralong anti-dehydration lifespan of 8 months.
- The DIH shows durable low ice adhesion, anti-frost and anti-freezing properties.

Graphic Abstract

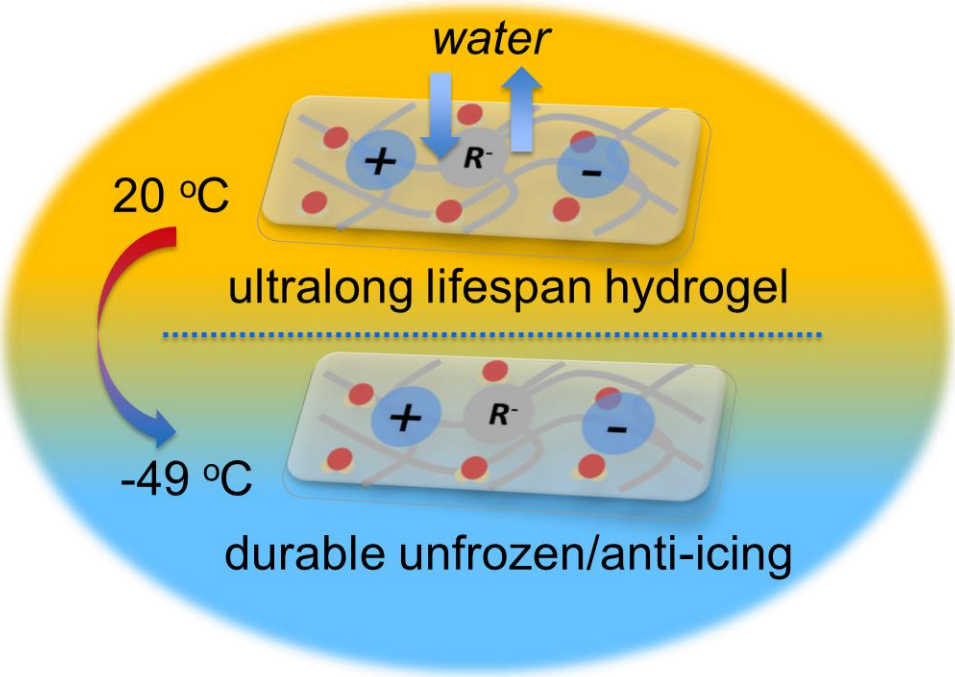

Dual-Ionic Hydrogels with Ultralong Anti-dehydration Lifespan and Superior Anti-icing Performance

Tong Li[a1*], Ke Xu[b1], Lianxin Shi[c], Jianyang Wu[b*], Jianying He[d] and Zhiliang Zhang[d]

[a]Zhejiang Key Laboratory of Marine Materials and Protective Technologies, Key Laboratory of Marine Materials and Related Technologies, Ningbo Institute of Materials Technology and Engineering, Chinese Academy of Sciences, Ningbo 315201, China.

[b]Department of Physics, Research Institute for Biomimetics and Soft Matter, Fujian Provincial Key Laboratory for Soft Functional Materials Research, Xiamen University, Xiamen 361005, PR China.

[c]CAS Key Laboratory of Bio-inspired Materials and Interfacial Science, CAS Center for Excellence in Nanoscience, Technical Institute of Physics and Chemistry, Chinese Academy of Sciences, Beijing 100190. China.

[d]NTNU Nanomechanical Lab, Department of Structural Engineering, Norwegian University of Science and Technology (NTNU), Trondheim 7491, Norway.

[1]These authors contributed equally to this work

[*]E-mail: tong@nimte.ac.cn, jianyang@xmu.edu.cn

Abstract:

Water-rich hydrogels find a wide range of promising applications due to their combined solid/liquid-like properties. However, hydrogels often exhibit a short lifespan and suffer from functional failure due to water depletion via rapid evaporation and icing/freezing under low temperatures. To tackle these challenges, here we developed a Ca^{2+} and hydrophilic bonded $-SO_3^-$ group-based dual-ionic hydrogel (DIH) which possesses an ultralong anti-dehydration lifespan and outstanding anti-icing properties. The as-developed DIH can keep wet and flexible as its initial state for longer than 8 months in practical room environment (15-35 ºC, relative humidity of 30-90%), and show low ice adhesion of 2.3 kPa and durably frost-free property at -10.0 ℃ as well as anti-freezing property down to -49.0 ℃. According to the molecular dynamic simulations and experimental results, the superior anti-dehydration performances are due to the low-diffusion and high absorption capacity and self-replenishment of water via the dual-ionic strategy; the sufficient anti-icing Ca^{2+} result in the extremely low melting point and anti-icing properties of the DIH. This design sheds new light on developing next-generation durable hydrogels with applications in soft materials and functional surfaces under harsh conditions of both low humidity and low temperatures.

Keywords: dual-ionic hydrogel, anti-dehydration, anti-icing, anti-frost, long lifespan

1. Introduction

Hydrogels are a network of cross-linked polymer chains with hydrophilic groups containing a large amount of water/fluid in the matrix. A large amount of water/fluid in the polymer matrix enables hydrogels to show liquid-like properties. In contrast, the structural integrity of the polymer skeleton by chemical cross-links in hydrogels is insoluble in water, enabling it to hold a specific shape like solid[1-2]. Due to the inner fluidity and solidity, hydrogels are mechanically soft/flexible materials with liquid layers on surfaces, ensuring a variety of applications such as soft materials/devices and repellent surfaces (e.g. anti-icing/anti-adhesion surfaces)[3-8]. However, most hydrogels show short lifespans and failure of liquid-like and soft functionalities because of rapid loss of water and/or freeze at subzero temperature[9-10].

The rapid loss of water from hydrogel originates from the inherent difference in osmotic pressure between hydrogel and atomosphere[11]. It was reported that there is around 95% water lost from a physically cross-linked PVA hydrogel after 190 h at room temperature (RT) as a result of water evaporation [12], resulting in a rigid and dry state of PVA hydrogel. On the other hand, the freezing or icing of hydrogels causes loss of softness, flexibility or surficial functions in cold regions and winter[13] In the cold environment, ice formation and accretion lead to great difficulty in designing durable anti-icing and anti-freeze surfaces that can face diverse icing scenarios. For example, ice forms and accretes on frozen hydrogel, isolating hydrogel from objectives[7-8]. Consequently, to mitigate or overcome dehydration and/or icing/freezing, several strategies have been developed, including chemically bonding of hydrophobic elastomer layer (hydrogel-elastomer hybrids)[11, 14], organohydrogels[3, 13, 15-17] and electrolyte hydrogels (ionic hydrogels)[4, 18-19]. For example, by covalently bonding thin elastomer films on hydrogels, the hydrogel-elastomer hybrids can exhibit less weight variation in comparison with the counterpart, improving the effective anti-dehydration properties of hydrogels[11]. Moreover, their anti-dehydration and anti-freezing properties can be further enhanced by the introduction of ions

into the aqueous phase of hydrogel-elastomer hybrids[4]. To the best of the authors' knowledge, the water retention of the state-of-the-art hydrogel-elastomer hybrids can be achieved as around 70% after 6 days[14]. Unfortunately, the hydrogel-elastomer hybrids then lose the surficial liquid-like functions. By introducing the organic solvents with hydroxyl groups, hydrogels can improve the anti-dehydration and anti-icing properties because of organic solvent's low depletion speed and inhibition of ice nucleation[3, 20]. Furthermore, the organohydrogels, formed by the replacement of water in hydrogel with organic hydrophilic solvents, can result in a durable lifespan with anti-icing functions[13, 21]. However, the aqueous properties of the hydrogels were compensated. It is a grand challenge to develop durable aqueous hydrogels with a liquid-like surface.

Alternatively, the electrolyte hydrogels with a liquid-like performance have been developed to enhance water retention and/or depress freezing/icing without the sacrifice of the aqueous functions. These include hydrogels either bonded with ionic groups or infused with ions (salt). Although the bonded ionic groups could strongly enhance the hydrophilicity to prompt the water capture ability from atomosphere[22-23], drying still occurs and the reduction in freezing temperature is negligible due to extremely low content of bonded ionic groups in contrast to the high content of water. However, the ions (salt)-infused hydrogels are promising materials that show anti-dehydration and anti-icing functionalities due to the hygroscopicity and adjustable freezing temperature of salts[18, 24]. To date, the salts such as NaCl, LiCl, KCl and $CaCl_2$ have been utilized to prepare salt-infused hydrogels[7, 18]. A hydrogel prepared from 12 M LiCl shows excellent water retention, with a cumulative water loss of 11% after 5 days (RH 20%)[18], outperforming abovementioned hydrogels. Recently, a highly stretchable and tough hydrogel was developed to survive at low temperatures down to -57 °C[24], however, its durability such as water retention remains unknown yet. More recently, a sustainable NaCl-infused hydrogel was fabricated to show multi-functional anti-icing properties[7], in which the durability of the anti-icing properties was maintained by replenishment of salted water. However, the

ions-infused surface is prone to condense water droplets in the cold environment[7], leading to the dilution of ions. In practical applications, the evaporation of water from hydrogels and freezing/icing at low temperatures seemed to be inevitable, and this leads to the loss of unique mechanical softness, fluidity and flexibility of hydrogels. Hydrogels with long-term anti-dehydration and anti-icing properties at low temperatures are yet to be developed.

As is known, the Antarctic bacterium *Marinomonas primoryensis* survives in harsh conditions due to the production of Ca^{2+}-dependent antifreeze proteins (AFP), which depends on Ca^{2+} for antifreeze activity[25]. In addition, the $CaCl_2$ is a promising chemical to store water due to its strong hygroscopicity[26]. Inspired by those, herein we address the problems of rapid drying and freezing/icing at subzero temperatures by using the so-called double ions (free Ca^{2+} and bonded $-SO_3^-$) approach to develop dual-ionic hydrogel (DIH) with excellent anti-dehydration (non-drying) and anti-icing properties. The DIH was fabricated by infusing high hygroscopic $CaCl_2$ into the hydrogels that are covalently bonded with ionic groups. We demonstrated that the DIH can be durably stored without obvious morphology and properties change for at least 8 months in room environment, and can survive at temperatures down to -49.0 °C without freezing/icing. Anti-icing tests, surface wettability investigation and molecular dynamic (MD) simulations were adopted to reveal the physical insights underlying the excellent anti-dehydration and anti-icing properties.

2 Results and discussion

2.1 Design, fabrication and characterization of DIH

Figures 1a and b show the schematics of DIH in comparison with ions-free hydrogel, hydrogel bonded with ionic groups and ions (salt)-infused hydrogel. The traditional hydrogels like PVA hydrogel, NaCl-infused hydrogels show weak ability of water retention, being dried after several hours to days[7]. The ions-free hydrogels and hydrogels bonded with ionic groups freeze at subzero degrees as well as icing on their surfaces[7, 18], failing solid/liquid-like functionality. By utilization of the hygroscopic and anti-

freezing $CaCl_2$ and self-replenishment via bonded ionic groups, we propose using conflicting double ions to develop DIH that can survive at harsh subzero temperatures and variable relative humidity (RH), as shown by Figure 1b. In detail, the bonded ionic groups (R^-), homogeneously dispersed on polymer matrix, can enhance the inner and surficial hydrophilicity of hydrogel, endowing easy water capture and fast transportation speed of DIH[27-29]; the introduction of hygroscopic free ions (salt) in the hydrogels can prevent water from quick evaporation, inhibit ice nucleation and decrease water freezing point to extremely low temperature[30].

Figure 1c-e shows the schematic of the fabrication process of the DIH. Initially, *κ*-carrageenan (*κ*-CG) is dissolved in water. Then, glutaraldehyde is added to chemically crosslink the *κ*-CG catalyzed by hydrochloric acid. After that, the as-prepared sample is soaked into the calcium chloride aqueous solution with a concentration of 30 wt% for replacement of the pure water by $CaCl_2$ solution in the hydrogel. Finally, the DIH is obtained and stored in the calcium chloride aqueous solution to reach stability for the following structural characterization. In this study, PVA hydrogel, κ-CG hydrogels, NaCl (or $CaCl_2$) - infused PVA (or κ-CG) hydrogels are used for comparison with the DIH in this work. Attenuated total reflection infrared (ATR-IR) and Raman spectroscopy were performed to reveal the existing configuration of water molecules inside the DIH. As shown in Figure S1, the DIH has similar IR and Raman spectra to the 30 wt% $CaCl_2$ solution. In comparison to the IR spectra of *κ*-CG hydrogel and water, there is a significant decrease in the IR peak (−OH) of DIH at about 3270 cm^{-1}. In the Raman spectra, the peak (symmetric −OH stretch) shifts from about 3395 cm^{-1} to about 3437 cm^{-1}, and the shoulder peak (3244 cm^{-1}, asymmetric −OH stretch) decreases remarkably in comparison to the Raman spectra of *κ*-CG hydrogel and water. Those results indicate that the molecular configuration of water is strongly influenced by the ions in the DIH, and it shows physical properties (e.g. melting and freezing points) similar to the $CaCl_2$ aqueous solution.

The morphology and structure of DIH are investigated in comparison with the PVA hydrogel, κ-CG

hydrogel, 30 wt % $CaCl_2$-infused PVA hydrogel, 20 wt% NaCl-infused PVA hydrogel and 20 wt% NaCl-infused κ-CG hydrogel (Figures S2-4). Figure S2 shows the microphotographs of the surface of hydrogels. As is seen, abundant liquid layer appears on the DIH surface, similar to the case of the κ-CG and κ-CG-NaCl hydrogels. In contrast, the hydrogels prepared from PVA with/without ions hold small isolated droplets on their surfaces, indicating that the hydrogels with bonded ionic groups show better hydrophilicity than those without bonded ionic groups. Figures S3 and S4 show the top-view and cross-sectional images of the hydrogels after freeze-drying. The κ-CG and PVA hydrogels have clear surface morphologies with inner nanoporous structures. Instead, all the samples are covered by abundant salt on their surfaces, of which NaCl is easier to aggregate than $CaCl_2$. This indicates that Ca^{2+} is much harder to remove from the DIH matrix. The cross-sectional SEM images further demonstrate that salt aggregation appears inside the PVA-NaCl, PVA-$CaCl_2$ and κ-CG-NaCl samples. By comparison, the salt is homogeneously distributed inside the DIH sample (Figure S4c, the dark part is due to the hydrogel without drying out), indicating a strong interaction between Ca^{2+} and DIH hydrogels. Moreover, the mechanical responses of those hydrogels are investigated. Figure S5 compares their mechanical stress-strain curves. As is seen, there are significant differences in the stress responses between the hydrogels. The ultimate strength of DIH increases greatly after adding Ca^{2+} in contrast to the κ-CG.

2.2 Anti-dehydration and water self-replenishment of DIH.

To demonstrate the durable anti-dehydration performance, the variations in the normalized weight with time of DIH are recorded, as well as other common hydrogels (Figure 1a) for comparison. The weight of all investigated samples, including PVA hydrogel, *κ*-CG hydrogel, 30 wt% $CaCl_2$-infused PVA hydrogel, 20 wt% NaCl-infused PVA hydrogel, 20 wt% NaCl-infused *κ*-CG hydrogel and DIH, as a function of time under a RH of 50% at RT, are shown in Figure 2a. It's worth noting that the DIH indicates the *κ*-CG hydrogel infused with 30 wt% $CaCl_2$ without special explanation in the following

tests. The DIH loses its weight of *ca.* 13% within the initial 12 h, while there is negligible variation in the weight from 12 to 72 h. Within this period, the DIH maintains soft, wet and reconfigurable. For $CaCl_2$-infused PVA hydrogel, although there is similar tendency in water loss to the DIH, namely, a rapid loss of weight within the initial 12 h followed by a constant weight from 12 to 72h, the weight loss reached *ca.* 22% that is significantly higher than that of the DIH. What is worse, the other hydrogels (PVA hydrogel, *κ*-CG hydrogel, 20 wt% NaCl-infused PVA hydrogel and 20 wt% NaCl-infused *κ*-CG hydrogel) lost more than 35 wt% after 12 h. For example, the 20 wt% NaCl-infused PVA/*κ*-CG hydrogels lost weight of about 37% and 77%, respectively. In particular, the PVA hydrogel and *κ*-CG hydrogel quickly lost weight of over 80% within the initial 12 h and finally dried out after 24h. Figure S6 shows their images after storage of 24 h. As is indicated, they are rigid, opaque structures and are completely failed of the softness and liquid-like properties. Furthermore, the reasons for the anti-dehydration (water loss) differences among these hydrogels are discussed. On the basis of the results from Figure 2a and previous reports[31-32], Ca^{2+} shows a stronger water storage ability than Na^+, and the NaCl-infused hydrogels do not show anti-dehydration properties (Figure 2a). Hence, the water loss of hydrogels with Na^+ is much larger than hydrogels with Ca^{2+}. In addition, the *κ*-CG and PVA hydrogels have a water content of 98.0 and 90.9 wt %, respectively, thereby resulting in that the water loss of (NaCl-infused) *κ* -CG hydrogels is larger than (NaCl-infused) PVA hydrogels after the test. Figure 2b shows the long-term (25 days) weight changes of DIH to examine the durability in comparison with *κ*-CG hydrogel. Apparently, there is negligible change in weight of the DIH from 24 to 1500 h and the inset clearly shows the transparent and flexible properties of long-term DIH, demonstrating the long-term durability of DIH. Moreover, the sample of DIH was stored for 8 months (from Dec/2020 to July/2021) in the practical environment at RH of *ca.* 30-90% and ca. 25 ℃(±10 ℃), and it was found that as-stored DIH remains wet, flexible, transparent and soft, indicating its extremely lifespan for practical important applications.

Figure 2c and Table S1 compare the lifespan of investigated hydrogels and previously reported elastomers including ions-free hydrogels[11, 13, 33], organohydrogels[13, 15, 33], elastomer-hydrogels hybrid[11, 19, 34], hydrogels bonded with ionic groups, free ions-infused hydrogels[35] and dual ionic hydrogels at environmental conditions of RH of ca. 50 ±10 % and about room temperature. Herein, the lifespan is defined by the period in which a hydrogel becomes structurally rigid or dry. It should be noted that the lifespans of some references without the dry/rigid information are estimated by the weight loss ratio of the samples exceeding ca. 50%. The lifespans of PVA, *κ*-CG, NaCl-infused PVA and NaCl-infused *κ*-CG hydrogel hydrogels are around 9, 12, 6, and 6 h, respectively from the current work. For the $CaCl_2$-infused PVA hydrogel, because it gradually degrades after storage for 5 days, and it broke into pieces when it was bent, the lifespan of $CaCl_2$-infused PVA hydrogel is hard to define by the proposed rules as for the other hydrogels. In contrast to the hydrogels, salt-infused hydrogels, organohydrogels and the hydrogels bonded with ionic groups from the references, a DIH prepared from *κ*-CG-$CaCl_2$ shows an extreme lifespan of over 240 days, demonstrating high-performance durability. In addition, the dual-ionic hydrogels with different free ions are compared in Figure 2c (red part). The DIH with Ca^{2+} shows much better anti-dehydration durability (> 240 days) than that with Na^+ (6 h), indicating that Ca^{2+} is a good feed candidate for anti-dehydration.

As is known, the environmental RH is a key parameter that influences the evaporation of water from hydrogels. Figure 2d shows the variation in the normalized weight of the DIH with time under RHs of 30%, 50% and 70% at RT. Under RHs of 30% and 50%, the DIH loses its weight under a RH of 30% as a result of water evaporation, whereas under a high RH of 70%, it gains weight as a result of water absorption from the atmosphere. As the place time is over the critical values, all samples remain constant weight under the three different RHs due to the balance of water evaporation and absorption. The results indicate that the DIH can reach an equilibrium state under certain RH, before which the DIH absorbs water from the atmosphere under high RH (≥70%) and lose water to the

atmosphere under low RH (≤50%).

To reveal the self-replenishment of water, the DIH was placed under periodically alternating RHs of 30% and 70% with a period of 24 h at RT. Figure 2e shows the variation in the weight of DIH with time. As it can be seen, there is an apparent characteristic saw-tooth pattern in the weight-time curve. The weight of DIH decreases to *ca.* 70% of its initial weight after storage in low RH of 30%, while it roughly recovers to its initial weight after being stored to the RH of 70%. Remarkably, under RH of 70%, it is observed a thin layer of liquid on the surface of the DIH, indicating strong water capture ability. To further demonstrate the water self-replenishment property, DIH was freeze-dried to remove free water, followed by storage at RT with a RH of 50%. Figures 2f and S7 show the variation in the normalized weight of as-freeze-dried DIH and $CaCl_2$-infused PVA hydrogel with time at conditions of 50% RH and RT, as well as the images of as-freeze-dried DIH at two different time stages. After freeze-drying, DIH loses *ca.* 62% weight and becomes opaque and rigid as indicated by the inset. When as-freeze-dried DIH was stored at RT with RH of 50%, however, its weight significantly increases about 57% within 12 h followed by a negligible change in the weight from 12 to 72 h, in which as-freeze-dried DIH gradually changes to be transparent and flexible after 72 h. It is noted that, due to the collapse of the hydrogel structure during freeze-drying, the weight of as-freeze-dried DIH did not recover to its initial weight. In contrast, there is negligible change in the weight of freeze-dried $CaCl_2$-infused PVA hydrogel as it was placed under conditions of RT and RH of 50%, indicating its poor self-replenishment of water. The bonded $-R^-$ that homogeneously dispersed in DIH contribute to the self-replenishment of water by comparing the chemical composition difference between DIH and $CaCl_2$-infused PVA hydrogel.

In addition, the simultaneous thermal analysis consisting of thermogravimetric (TG) and Differential thermal analysis (DTA) was performed to evaluate the DIH in comparison with pure water, *κ*-CG hydrogel and 30 wt% $CaCl_2$ solution (**Figure S8**). It is observed that, for pure water and κ-CG

hydrogel systems, there is a significant loss of water below *ca.* 100 ℃ due to evaporation. However, for 30 wt% $CaCl_2$ solution and DIH systems, confined/bonded water loss occurs above 100 ℃. At the temperature of less than 95.6 ℃, the loss of weight for DIH is mainly dominated by evaporation of free water, whereas above 95.6 ℃, the loss of weight of DIH is dominated by the loss of confined/bonded water, indicating strong capability in water retention of the DIH. In a nutshell, DIH shows excellent anti-dehydration property due to its low water evaporation and strong self-replenishment of water.

2.3 Mechanisms of anti-dehydration and water self-replenishment

The molecular mechanisms underlying the durable anti-dehydration and water self-replenishment properties are mainly attributed to the synergistic actions of the hydrophilic bonded R^- and free Ca^{2+} (Figure 3a). The sufficient Ca^{2+} in the DIH could mitigate water evaporation and retain water in long-term due to the strong hygroscopicity of $CaCl_2$.[36] In addition, it is more energetically-favorable for water vapor and small water droplets nucleating on more hydrophilic surfaces compared to less hydrophilic ones,[37-39] thereby that water could be more easily captured from the atmosphere by more hydrophilic DIH than less hydrophilic hydrogels (Figure 3k). Here, molecular dynamics (MD) simulations are conducted to understand the anti-dehydration of DIH in comparison with other kinds of hydrogels (Figure 1a). Figure 3b shows the perspective-viewed MD model in which the linear polymer chain of DIH is surrounded by different liquids (water, NaCl solution or $CaCl_2$ solution). As shown in Figure 3c, the models used in the MD simulations include water, Na^+ and Ca^{2+} infused hydrogels without bonded ionic groups ($-SO_3^-$), as well as water, Na^+ and Ca^{2+} infused hydrogel bonded with ionic groups ($-SO_3^-$), respectively.

Figure 3d shows the mean square displacement (MSD) of water molecules of various hydrogels with and without bonded ionic groups. As it can be observed, the MSD curves of water molecules in Ca^{2+} infused hydrogels are obviously below those of other hydrogels, demonstrating low diffusivity of water in Ca^{2+} infused hydrogels. This indicates that the Ca^{2+} could strongly reduce the mobility of

water molecules in Ca^{2+} infused hydrogels, resulting in inhibition of water evaporation, thereby explaining that the Ca^{2+} infused hydrogels show a much longer lifespan in water retention (Figure 1c). By contrast, the water and Na^{+} infused hydrogels exhibit high MSD of water molecules, indicating a faster speed of water evaporation. In addition, Figures 3e-j show the iso-density contour plots of water in different hydrogels with/without $-SO_3^-$. As is seen, water molecules are homogeneously dispersed in water/Na^{+} infused hydrogels, while water molecules in Ca^{2+} infused hydrogels with/without $-SO^{3-}$ are heterogeneously distributed, for example, there is an apparent aggregation of water molecules around polymer chain. Such aggregation of water molecules in Ca^{2+} infused hydrogel limits the mobility of water molecules, thereby inhibiting water evaporation. In Figure S9, the iso-density contour plots of Na^{+} and Ca^{2+} in hydrogels with and without $-SO_3^-$ also reveal that the Ca^{2+} ion tends to aggregate, indicating the inhibition of the mobility and evaporation of water via the Ca^{2+} domain.

Figure 3k compares the wettability of DIH with the other hydrogels (PVA hydrogel, *κ*-CG hydrogel, 30 wt% $CaCl_2$-infused PVA hydrogel, 20 wt% NaCl-infused PVA hydrogel and 20 wt% NaCl-infused *κ*-CG hydrogel). As it can be observed, the water contact angle (WCA) is close to 0^o on the surface of DIH and 20 wt% NaCl-infused κ-CG hydrogel, indicating their superhydrophilic property. However, the *κ*-CG hydrogel, 20 wt% NaCl-infused PVA hydrogel and $CaCl_2$-infused PVA hydrogel has a WCA of around 9.3^o, 69.4^o and 44.6^o, showing less hydrophilic than the DIH. By comparison, there is a more significant reduction in WCA for the hydrogels with bonded ionic groups than for salt-infused hydrogels, in which the hydrophilic R^- ($-SO_3^-$) groups are homogeneously dispersed in the polymer chains of hydrogels and enable more hydrophilic surfaces than those without hydrophilic groups. Hence, the superhydrophilicity of DIH enables much easier water nucleation and capture on its surface than the less hydrophilic ones, as a result of self-replenishment of water for durability.

2.4 Anti-icing properties

The anti-freezing behavior of DIH and the anti-icing properties of its surface are investigated by DSC, ice adhesion, anti-frost and droplet freezing tests. As shown in Figure 4a, the melting points of both the DIHs and $CaCl_2$ solutions decrease with the increase of the solution concentration. This suggests that the anti-freezing properties of the DIHs can be regulated on the basis of the melting points of the $CaCl_2$ solution. Intriguingly, the lowest melting point of the DIH prepared with 30 wt% $CaCl_2$ can be down to -49.0 ℃ based the DSC curve (Figure 4b). It's worth noting that the DIH indicates the κ-CG hydrogel infused with 30 wt% $CaCl_2$ without special explanation in the following tests. Figures 4c and d show the schematic of the ice adhesion test and the corresponding cyclic ice adhesion strength, respectively. In contrast to *κ*-CG hydrogel with high ice adhesion of 925.0 ± 59.4 kPa, the DIH yields extremely low ice adhesion of less than 2.3 kPa during 25 icing/deicing cyclic tests, demonstrating durable anti-icing performance. This is because there is a liquid wet layer on the surface of ice as shown in the inset of Figure 4d, which serves as the lubricating layer, thereby resulting in very low ice adhesion [40]. In comparison with the representative anti-icing superhydrophobic surfaces (SHS; PDMS)[41], slippery-liquid-infused porous surface (SLIPS; Si-oil)[41] with an obvious increase of the ice adhesion after 15 icing/deicing cyclic tests, the ice adhesion of DIH does not change obviously after 25 icing/deicing cyclic tests; the durability of DIH is also competitive to the durable anti-icing soft slippage surface (PDMS silane)[42], demonstrating the anti-icing durability of DIH.

In addition, DIH exhibits durable anti-frost properties. As indicated by Figure 4e, there is no frost formation on the surface of as-fabricated DIH at -10 ℃ and RH of *ca.* 50% for 30 min, while frost forms on the glass surface and κ-CG hydrogel freezes within 1 min. As shown in Figure S10, the normalized transmittance of the DIH does not change during the 30 min test, indicating no frost formation during the test. However, the glass surface is gradually covered with frost and the normalized transmittance decreases to ca.70 % after 30 min; the κ-CG hydrogel freezes within 1 min and the normalized transmittance decreased to 0%. Furthermore, Figure 4f shows no frost formation

on the DIH surface after 8 h in comparison with the Al plate covered with white frost within 2 min at -10 ^{o}C (stage temperature) and a RH of *ca*. 50% (environmental temperature: 23 ^{o}C). It should be noted that the anti-frost test has to be terminated after 8 h due to the limitation of a batch supply of the liquid N_2, but it is believed that the DIH surface can show anti-frost performance over 8 h. In addition, the DIH is coated on the lens to demonstrate its practical anti-frost applications. The samples were stored in -20 ^{o}C for 30 min and then moved to the environment with a RH of ca. 50% at room temperature. As shown in Figure 4g, the surface of the lens with DIH has no frost formation with a transparent property, while the pristine lens is covered with frost and lost transparency within 1 min. Figure 4h shows the freezing time of water droplets on the surface of different hydrogels at -10 ℃ to reveal the droplet freezing behavior. It is observed that when a water droplet of a volume of 4 uL is deposited on the DIH surface, it quickly spreads on the DIH surface with a superhydrophilic property. Interestingly, there is no ice formation on the surface of the as-fabricated after 3h, revealing a long-term freezing delay time. By contrast, the deposited water droplets freeze on the glass and κ-CG surfaces after *ca.* 54.0 s and 9.5 s, respectively. The remarkable anti-frost property and long freezing delay time are primarily ascribed to surficial superhydrophilicity and inhibition of ice nucleation via ions of DIH, as illustrated in Figures 4i and S11. The superhydrophilicity inhibits droplet formation on the surface, and the anti-freezing free Ca^{2+} inhibits the ice formation, as demonstrated in Figures 3k and 4a. When the droplet contacts the DIH surface, it quickly spreads on the surface forming an unfrozen thin liquid layer, in which water also evaporates from the surface to reach an equilibrium. In contrast, droplets accrete on the surface (e.g. anti-icing ions-infused hydrogel) without superhydrophilicity, leading to the damage of the surface optical properties (Figure S11a). In addition, to demonstrate the durable anti-icing properties, the anti-frost test shows no frost forms on the DIH after storage for 8 months. Hence, it is predicted that the DIH surface could durably avoid ice formation in the long term due to the inherent extremely low melting point (Figure 4b).

3 Conclusions

To overcome the well-known challenges of the high-performance anti-icing hydrogel materials, DIH is developed to realize the durable anti-dehydration function, anti-freezing and anti-icing properties, which contains sufficient free ions and bonded ionic groups. The as-developed DIH shows excellent ability of water retention for at least 8 months in room environment and can survive low temperatures down to -49.0 °C without freezing. Moreover, it shows extremely low ice adhesion strength down to 2.3 kPa, durable anti-frost property, as well as long-term droplet freezing delay time. Molecular dynamics simulation and experimental characterizations suggest that the mechanism of the durable anti-dehydration property is attributed to the synergistic actions (water capture and storage) of the bonded R^- and free Ca^{2+}, and the anti-freezing and anti-icing properties are attributed to the inhibition of ice formation by ions and the surficial superhydrophilicity. This work provides a new avenue for long-term hydrogel that can survive in harsh conditions of low-temperature and various RH.

Supporting Information

The Supporting Information is available free of charge on the website. Materials and methods, molecular dynamics simulations details.

Acknowledgments

This work was financially supported by the National Natural Science Foundation of China (Nos. 12002350, 12172314 and 11772278) and the Open Funding of the CAS Key Laboratory of Bio-inspired Materials and Interfacial Science, Technical Institute of Physics and Chemistry. The Research Council of Norway is acknowledged for the support to the PETROMAKS2 Project Durable Arctic Icephobic Materials (No. 255507) and the Dual-Functional Anti-Gas Hydrate Surfaces (Dandra, No. 302348). The supercomputer CPU hours were provided by the Norwegian Metacenter for Computational science (Project ID: NN9110K and NN9391K).

References

(1) Liu, X. Y.; Liu, J.; Lin, S. T.; Zhao, X. H. Hydrogel machines. *Materials Today* **2020,** *36*, 102-124, DOI: 10.1016/j.mattod.2019.12.026.

(2) Guo, Y.; Bae, J.; Fang, Z.; Li, P.; Zhao, F.; Yu, G. Hydrogels and Hydrogel-Derived Materials for Energy and Water Sustainability. *Chem Rev* **2020,** *120* (15), 7642-7707, DOI: 10.1021/acs.chemrev.0c00345.

(3) Zhang, J. W.; Dong, D. D.; Guan, X. Y.; Zhang, E. M.; Chen, Y. M.; Yang, K.; Zhang, Y. X.; Khan, M. M. B.; Arfat, Y.; Aziz, Y. Physical Organohydrogels With Extreme Strength and Temperature Tolerance. *Front Chem* **2020,** *8* (102), 102, DOI: 10.3389/fchem.2020.00102.

(4) Zhao, X.; Chen, F.; Li, Y.; Lu, H.; Zhang, N.; Ma, M. Bioinspired ultra-stretchable and anti-freezing conductive hydrogel fibers with ordered and reversible polymer chain alignment. *Nat Commun* **2018,** *9* (1), 3579, DOI: 10.1038/s41467-018-05904-z.

(5) Tu, Y.; Chen, Q.; Liang, S.; Zhao, Q.; Zhou, X.; Huang, W.; Huang, X.; Zhang, L. Antifreezing Heat-Resistant Hollow Hydrogel Tubes. *ACS Appl Mater Interfaces* **2019,** *11* (20), 18746-18754, DOI: 10.1021/acsami.9b03892.

(6) Zhu, H.; Xu, B.; Wang, Y.; Pan, X.; Qu, Z.; Mei, Y. Self-powered locomotion of a hydrogel water strider. *Sci Robot* **2021,** *6* (53), eabe7925, DOI: 10.1126/scirobotics.abe7925.

(7) Li, T.; Ibanez-Ibanez, P. F.; Hakonsen, V.; Wu, J.; Xu, K.; Zhuo, Y.; Luo, S.; He, J.; Zhang, Z. Self-Deicing Electrolyte Hydrogel Surfaces with Pa-level Ice Adhesion and Durable Antifreezing/Antifrost Performance. *ACS Appl Mater Interfaces* **2020,** *12* (31), 35572-35578, DOI: 10.1021/acsami.0c06912.

(8) He, Z. Y.; Wu, C. Y.; Hua, M. T.; Wu, S. W.; Wu, D.; Zhu, X. Y.; Wang, J. J.; He, X. M. Bioinspired Multifunctional Anti-icing Hydrogel. *Matter* **2020,** *2* (3), 723-734, DOI: 10.1016/j.matt.2019.12.017.

(9) Zhou, D.; Chen, F.; Handschuh-Wang, S.; Gan, T.; Zhou, X.; Zhou, X. Biomimetic Extreme-Temperature- and Environment-Adaptable Hydrogels. *Chemphyschem* **2019,** *20* (17), 2139-2154, DOI: 10.1002/cphc.201900545.

(10) Jian, Y. K.; Handschuh-Wang, S.; Zhang, J. W.; Lu, W.; Zhou, X. C.; Chen, T. Biomimetic anti-freezing polymeric hydrogels: keeping soft-wet materials active in cold environments. *Materials Horizons* **2021,** *8* (2), 351-369, DOI: 10.1039/d0mh01029d.

(11) Yuk, H.; Zhang, T.; Parada, G. A.; Liu, X.; Zhao, X. Skin-inspired hydrogel-elastomer hybrids with robust interfaces and functional microstructures. *Nat Commun* **2016,** *7* (1), 12028, DOI: 10.1038/ncomms12028.

(12) Kudo, K.; Ishida, J.; Syuu, G.; Sekine, Y.; Ikeda-Fukazawa, T. Structural changes of water in

poly(vinyl alcohol) hydrogel during dehydration. *J Chem Phys* **2014,** *140* (4), 044909, DOI: 10.1063/1.4862996.

(13) Chen, F.; Zhou, D.; Wang, J.; Li, T.; Zhou, X.; Gan, T.; Handschuh-Wang, S.; Zhou, X. Rational Fabrication of Anti-Freezing, Non-Drying Tough Organohydrogels by One-Pot Solvent Displacement. *Angew Chem Int Ed Engl* **2018,** *57* (22), 6568-6571, DOI: 10.1002/anie.201803366.

(14) Liu, T.; Liu, M.; Dou, S.; Sun, J.; Cong, Z.; Jiang, C.; Du, C.; Pu, X.; Hu, W.; Wang, Z. L. Triboelectric-Nanogenerator-Based Soft Energy-Harvesting Skin Enabled by Toughly Bonded Elastomer/Hydrogel Hybrids. *ACS Nano* **2018,** *12* (3), 2818-2826, DOI: 10.1021/acsnano.8b00108.

(15) Xu, B.; Liu, Y.; Wang, L.; Ge, X.; Fu, M.; Wang, P.; Wang, Q. High-Strength Nanocomposite Hydrogels with Swelling-Resistant and Anti-Dehydration Properties. *Polymers (Basel)* **2018,** *10* (9), 1025, DOI: 10.3390/polym10091025.

(16) Shi, S. J.; Peng, X.; Liu, T. Q.; Chen, Y. N.; He, C. C.; Wang, H. L. Facile preparation of hydrogen-bonded supramolecular polyvinyl alcohol-glycerol gels with excellent thermoplasticity and mechanical properties. *Polymer* **2017,** *111*, 168-176, DOI: 10.1016/j.polymer.2017.01.051.

(17) Mo, F.; Liang, G.; Meng, Q.; Liu, Z.; Li, H.; Fan, J.; Zhi, C. A flexible rechargeable aqueous zinc manganese-dioxide battery working at −20 °C. *Energy & Environmental Science* **2019,** *12* (2), 706-715, DOI: 10.1039/c8ee02892c.

(18) Bai, Y. Y.; Chen, B. H.; Xiang, F.; Zhou, J. X.; Wang, H.; Suo, Z. G. Transparent hydrogel with enhanced water retention capacity by introducing highly hydratable salt. *Applied Physics Letters* **2014,** *105* (15), 151903, DOI: 10.1063/1.4898189.

(19) Le Floch, P.; Yao, X.; Liu, Q.; Wang, Z.; Nian, G.; Sun, Y.; Jia, L.; Suo, Z. Wearable and Washable Conductors for Active Textiles. *ACS Appl Mater Interfaces* **2017,** *9* (30), 25542-25552, DOI: 10.1021/acsami.7b07361.

(20) Gao, H.; Zhao, Z.; Cai, Y.; Zhou, J.; Hua, W.; Chen, L.; Wang, L.; Zhang, J.; Han, D.; Liu, M.; Jiang, L. Adaptive and freeze-tolerant heteronetwork organohydrogels with enhanced mechanical stability over a wide temperature range. *Nat Commun* **2017,** *8* (1), 15911, DOI: 10.1038/ncomms15911.

(21) Chen, F.; Xu, Z.; Wang, H.; Handschuh-Wang, S.; Wang, B.; Zhou, X. Bioinspired Tough Organohydrogel Dynamic Interfaces Enabled Subzero Temperature Antifrosting, Deicing, and Antiadhesion. *ACS Appl Mater Interfaces* **2020,** *12* (49), 55501-55509, DOI: 10.1021/acsami.0c17163.

(22) Aktas, D. K. Swelling and drying process in ionic hydrogels for low and high pH using fluorescence technique. *Proceedings of Pps-32: The 32nd International Conference of the Polymer Processing Society* **2017,** *1914* (1), 090007, DOI: 10.1063/1.5016753.

(23) Vogt, B. D.; Soles, C. L.; Lee, H. J.; Lin, E. K.; Wu, W. L. Moisture absorption and absorption

kinetics in polyelectrolyte films: influence of film thickness. *Langmuir* **2004,** *20* (4), 1453-1458, DOI: 10.1021/la035239i.

(24) Morelle, X. P.; Illeperuma, W. R.; Tian, K.; Bai, R.; Suo, Z.; Vlassak, J. J. Highly Stretchable and Tough Hydrogels below Water Freezing Temperature. *Adv Mater* **2018,** *30* (35), e1801541, DOI: 10.1002/adma.201801541.

(25) Garnham, Christopher P.; Gilbert, Jack A.; Hartman, Christopher P.; Campbell, Robert L.; Laybourn-Parry, J.; Davies, Peter L. A Ca2+-dependent bacterial antifreeze protein domain has a novel β-helical ice-binding fold. *Biochemical Journal* **2008,** *411* (1), 171-180, DOI: 10.1042/BJ20071372.

(26) Guo, L.; Gu, W.; Peng, C.; Wang, W.; Li, Y. J.; Zong, T.; Tang, Y.; Wu, Z.; Lin, Q.; Ge, M.; Zhang, G.; Hu, M.; Bi, X.; Wang, X.; Tang, M. A comprehensive study of hygroscopic properties of calcium- and magnesium-containing salts: implication for hygroscopicity of mineral dust and sea salt aerosols. *Atmospheric Chemistry and Physics* **2019,** *19* (4), 2115-2133, DOI: 10.5194/acp-19-2115-2019.

(27) Shimoaka, T.; Wakai, C.; Sakabe, T.; Yamazaki, S.; Hasegawa, T. Hydration structure of strongly bound water on the sulfonic acid group in a Nafion membrane studied by infrared spectroscopy and quantum chemical calculation. *Phys Chem Chem Phys* **2015,** *17* (14), 8843-9, DOI: 10.1039/c5cp00567a.

(28) Ashkani, M.; Bouhendi, H.; Kabiri, K.; Rostami, M. R. Synthesis of poly (2-acrylamido-2-methyl propane sulfonic acid) with high water absorbency and absorption under load (AUL) as concrete grade superabsorbent and its performance. *Construction and Building Materials* **2019,** *206*, 540-551, DOI: 10.1016/j.conbuildmat.2019.02.070.

(29) Bajpai, S. K.; Daheriya, P.; Ahuja, S.; Gupta, K. Water absorption and antimicrobial behavior of physically cross linked poly (vinyl alcohol)/carrageenan films loaded with minocycline. *Designed Monomers and Polymers* **2016,** *19* (7), 630-642, DOI: 10.1080/15685551.2016.1187444.

(30) Li, R.; Shi, Y.; Shi, L.; Alsaedi, M.; Wang, P. Harvesting Water from Air: Using Anhydrous Salt with Sunlight. *Environ Sci Technol* **2018,** *52* (9), 5398-5406, DOI: 10.1021/acs.est.7b06373.

(31) Zieger, P.; Väisänen, O.; Corbin, J. C.; Partridge, D. G.; Bastelberger, S.; Mousavi-Fard, M.; Rosati, B.; Gysel, M.; Krieger, U. K.; Leck, C.; Nenes, A.; Riipinen, I.; Virtanen, A.; Salter, M. E. Revising the hygroscopicity of inorganic sea salt particles. *Nature Communications* **2017,** *8* (1), 15883, DOI: 10.1038/ncomms15883.

(32) Vainio, E.; DeMartini, N.; Hupa, L.; Åmand, L.-E.; Richards, T.; Hupa, M. Hygroscopic Properties of Calcium Chloride and Its Role on Cold-End Corrosion in Biomass Combustion. *Energy & Fuels* **2019,** *33* (11), 11913-11922, DOI: 10.1021/acs.energyfuels.9b02731.

(33) Liu, B.; Li, F.; Niu, P.; Li, H. Tough Adhesion of Freezing- and Drying-Tolerant Transparent Nanocomposite Organohydrogels. *ACS Appl Mater Interfaces* **2021,** *13* (18), 21822-21830, DOI: 10.1021/acsami.1c04758.

(34) Jing, X.; Li, H.; Mi, H. Y.; Feng, P. Y.; Tao, X.; Liu, Y.; Liu, C.; Shen, C. Enhancing the Performance of a Stretchable and Transparent Triboelectric Nanogenerator by Optimizing the Hydrogel Ionic Electrode Property. *ACS Appl Mater Interfaces* **2020,** *12* (20), 23474-23483, DOI: 10.1021/acsami.0c04219.

(35) Zhao, Y. M.; Yan, Y. G.; Cui, X.; Wu, X. W.; Wang, H.; Huang, J.; Qiu, X. Y. A Conductive, Self-Healing Hybrid Hydrogel with Excellent Water-Retention and Thermal Stability by Introducing Ethylene Glycol as a Crystallization Inhibitor. *Colloids and Surfaces a-Physicochemical and Engineering Aspects* **2020,** *607*, 125443, DOI: 10.1016/j.colsurfa.2020.125443.

(36) Vainio, E.; Demartini, N.; Hupa, L.; Amand, L. E.; Richards, T.; Hupa, M. Hygroscopic Properties of Calcium Chloride and Its Role on Cold-End Corrosion in Biomass Combustion. *Energy & Fuels* **2019,** *33* (11), 11913-11922, DOI: 10.1021/acs.energyfuels.9b02731.

(37) Seo, D.; Lee, J.; Lee, C.; Nam, Y. The effects of surface wettability on the fog and dew moisture harvesting performance on tubular surfaces. *Sci Rep* **2016,** *6* (1), 24276, DOI: 10.1038/srep24276.

(38) Dai, X.; Sun, N.; Nielsen, S. O.; Stogin, B. B.; Wang, J.; Yang, S.; Wong, T.-S. Hydrophilic directional slippery rough surfaces for water harvesting. *Science Advances* **2018,** *4* (3), eaaq0919, DOI: 10.1126/sciadv.aaq0919.

(39) Parker, A. R.; Lawrence, C. R. Water capture by a desert beetle. *Nature* **2001,** *414* (6859), 33-34, DOI: 10.1038/35102108.

(40) Dou, R.; Chen, J.; Zhang, Y.; Wang, X.; Cui, D.; Song, Y.; Jiang, L.; Wang, J. Anti-icing coating with an aqueous lubricating layer. *ACS Appl Mater Interfaces* **2014,** *6* (10), 6998-7003, DOI: 10.1021/am501252u.

(41) Barthwal, S.; Lee, B.; Lim, S.-H. Fabrication of robust and durable slippery anti-icing coating on textured superhydrophobic aluminum surfaces with infused silicone oil. *Applied Surface Science* **2019,** *496*, 143677, DOI: j.apsusc.2019.143677.

(42) Golovin, K.; Kobaku, S. P.; Lee, D. H.; DiLoreto, E. T.; Mabry, J. M.; Tuteja, A. Designing durable icephobic surfaces. *Science Advances* **2016,** *2* (3), e1501496, DOI: 10.1126/sciadv.1501496.

Figures:

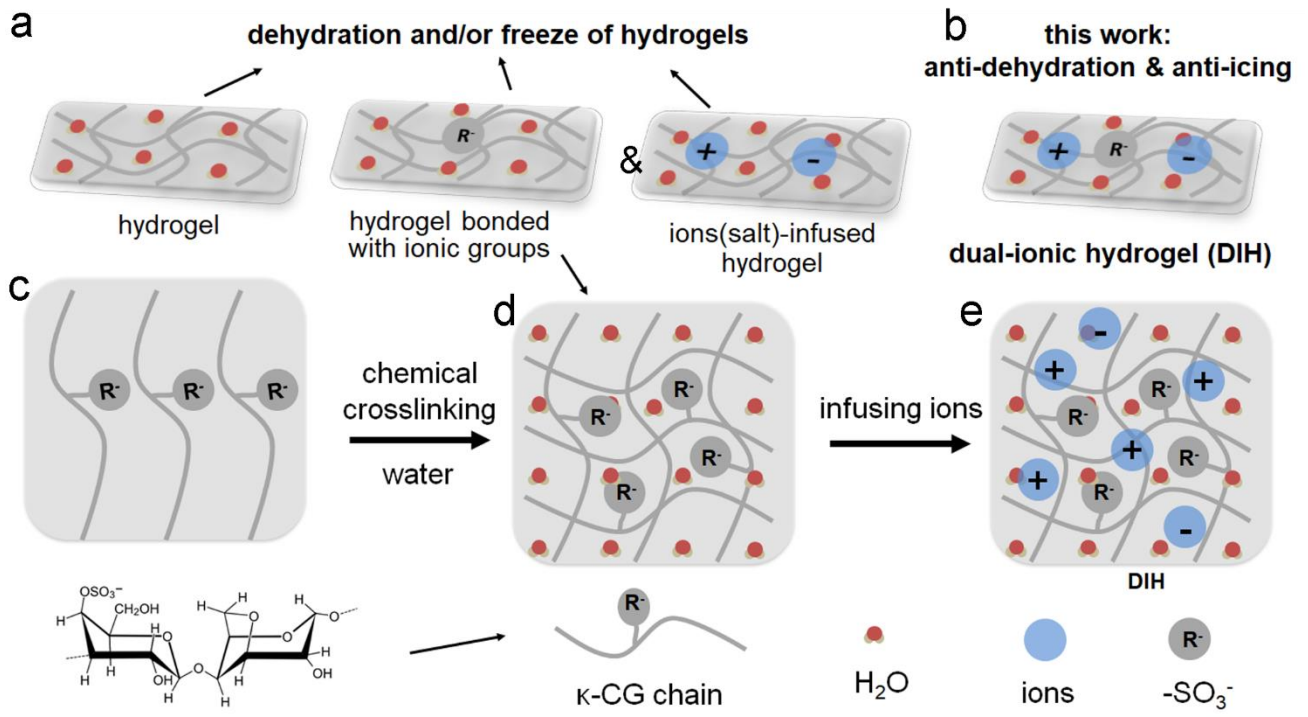

Figure 1 (a,b) Schematics of DIH in comparison with ions-free hydrogels, hydrogel bonded with ionic groups, ions (salt)-infused hydrogel and DIH. (c-e) Fabrication process of the DIH.

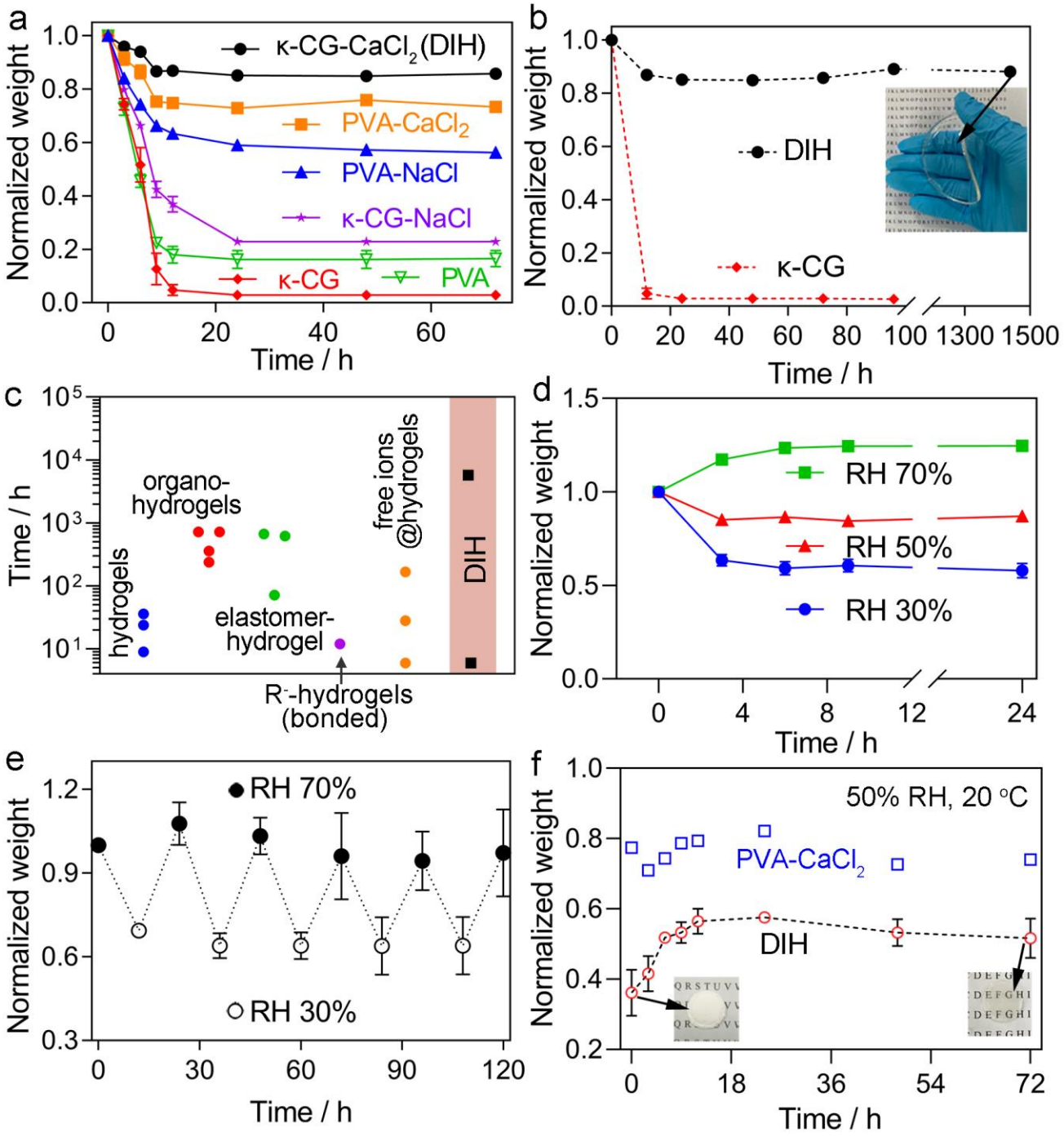

Figure 2 Anti-dehydration tests of various hydrogels. (a) Normalized weight changes of various hydrogels with time at RT with a RH of *ca.* 50%; (b) Normalized weight changes of DIH with time in the practical room environment at the temperature range of ca. 15-35 ºC with a RH of ca. 30-90%; the inset in (b) is the image of DIH after being stored for *ca.* 1500 h. (c) The lifespan of different kinds of hydrogels from our work and previous reports (ions-free hydrogels[11, 13, 33],

organohydrogels[13, 15, 33], elastomer-hydrogels hydbid[11, 19, 34], hydrogels bonded with ionic groups, free ions-infused hydrogels[35] and dual-ionic hydrogels). Normalized weight changes of DIHs with time at RT under (d) RH of 30%, 50% and 70%, respectively, and (e) alternative RH (30 to 70%), indicating the humidity-responsive and self-replenishment properties of DIH. (f) Normalized weight changes of freeze-dried DIH and $CaCl_2$-infused PVA hydrogel with time at 50% RH and RT, revealing the superior self-replenishment of DIH but non-self-replenishment of the hydrogel with free ions after they suffer from an extremely dry environment. The insets in (f) are the images of DIH after freeze-drying and self-replenishment of water for 72 h, respectively.

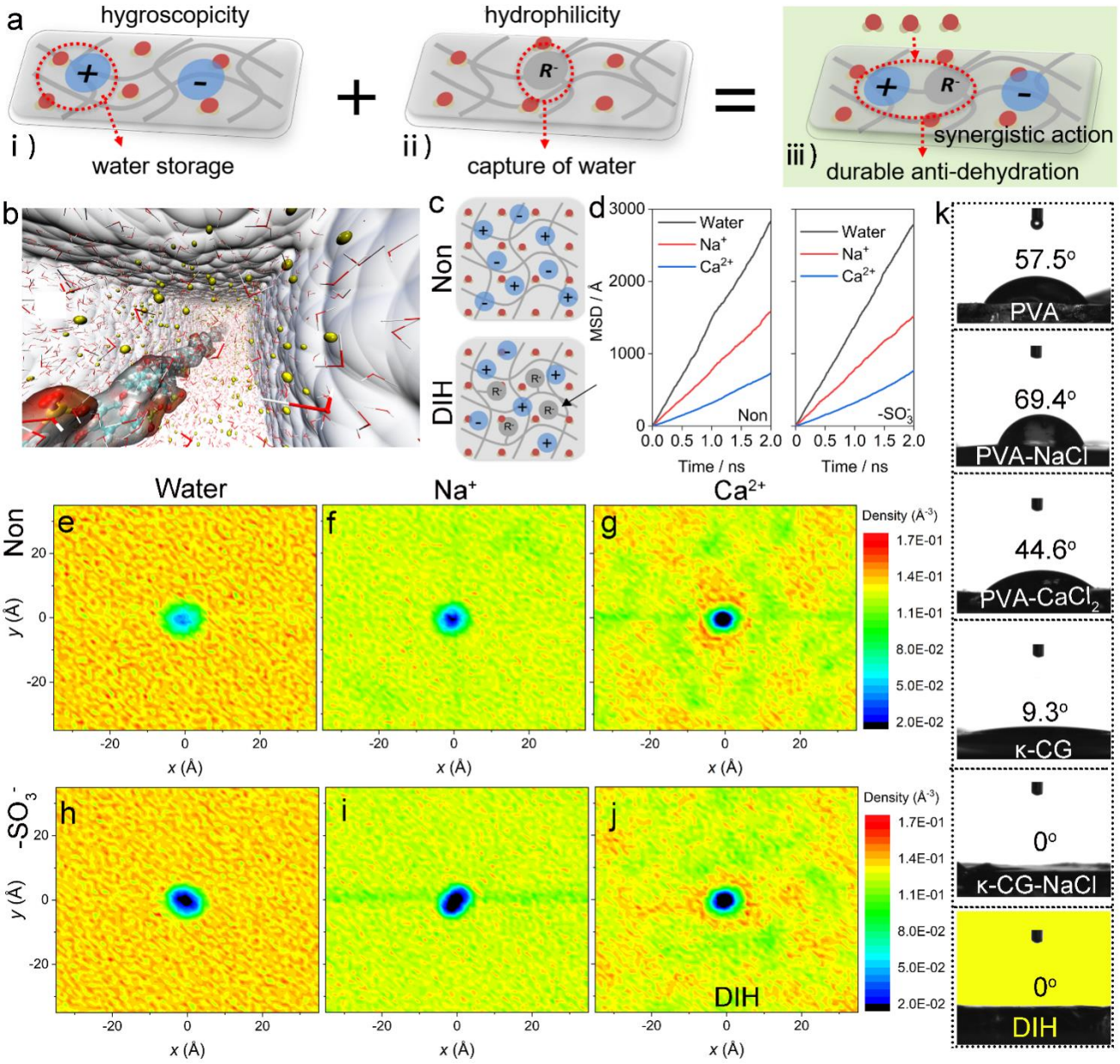

Figure 3 MD simulation and experimental investigation of the interaction between water and hydrogels. (a) Schematic of the assumed mechanism of the durable anti-dehydration property via hygroscopicity and hydrophilicity. (b) Schematic of the MD model. (c) Schematic of ion-infused hydrogel without bonded ionic groups and DIH. (d) Water molecules MSD (mean square displacement) of different solution-infused hydrogels bonded with/without $-SO_3^-$. (e-j) Density distribution of water in the different solution-infused hydrogels with/without $-SO_3^-$. In e-j, the circle in the center of density

distribution represents the approximate range of polymer chain motion. The density distribution of water molecules is related to the ions. (k) Water contact angles of DIH in comparison with other types of hydrogels.

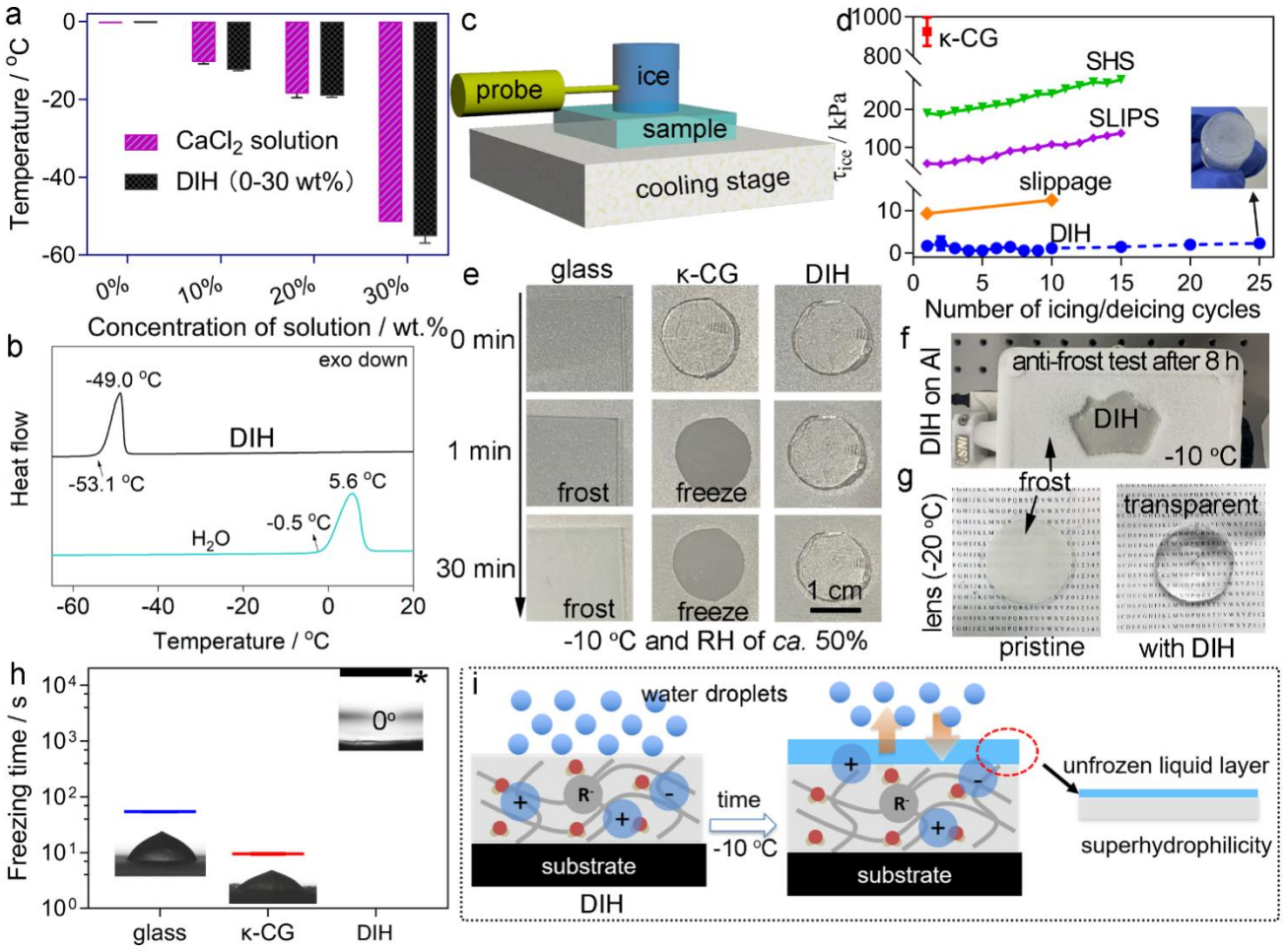

Figure 4 Anti-icing properties of DIH. (a) The melting temperature of DIHs prepared from variable concentrations of ions. (b) DSC curve of DIH in comparison to water. (c, d) Schematic of the method to test the ice adhesion and the corresponding ice adhesion strength of DIH during 25 icing/deicing cycles in comparison with superhydrophobic surfaces (SHS)[41], slippery-liquid-infused porous surface (SLIPS)[41] and the interfacial slippage surfaces[42]. The inset in (d) is the image of detached ice after the 25th icing/deicing cycle. (e-g) Anti-frost tests and (g) droplets freezing time of DIH in comparison to different surfaces. The insets in (h) are the side-view images of droplets on surfaces after freeze. The (*) in (h) indicates no ice forms on the DIH surfaces exceeding 10000 s. (i) Schematic of mechanism of the anti-frost property.

Declaration of interests

The authors declare that they have no known competing financial interests or personal relationships that could have appeared to influence the work reported in this paper.

Dual-Ionic Hydrogels with Ultralong Anti-dehydration Lifespan and Superior Anti-icing Performance

Tong Li[a1*], Ke Xu[b1], Lianxin Shi[c], Jianyang Wu[b*], Jianying He[d] and Zhiliang Zhang[d]

[a]Zhejiang Key Laboratory of Marine Materials and Protective Technologies, Key Laboratory of Marine Materials and Related Technologies, Ningbo Institute of Materials Technology and Engineering, Chinese Academy of Sciences, Ningbo 315201, China.

[b]Department of Physics, Research Institute for Biomimetics and Soft Matter, Fujian Provincial Key Laboratory for Soft Functional Materials Research, Xiamen University, Xiamen 361005, PR China.

[c]CAS Key Laboratory of Bio-inspired Materials and Interfacial Science, CAS Center for Excellence in Nanoscience, Technical Institute of Physics and Chemistry, Chinese Academy of Sciences, Beijing 100190. China.

[d]NTNU Nanomechanical Lab, Department of Structural Engineering, Norwegian University of Science and Technology (NTNU), Trondheim 7491, Norway.

[1]These authors contributed equally to this work

[*]E-mail: tong@nimte.ac.cn, jianyang@xmu.edu.cn

Materials and chemicals.

Sodium Chloride (NaCl, ≥99%), Calcium Chloride ($CaCl_2$, ≥96%), κ-Carrageenan (κ-CG), fully hydrolyzed poly(vinyl alcohol) (PVA, P1799), acetic acid (99%), glutaraldehyde solution (GA, 50 % in H_2O) and hydrochloric acid (37%) were purchased from Shanghai Aladdin Technology Co. Ltd (Shanghai, China). All chemicals were used without further purification. Ultrapure water with a resistivity higher than 15.0 MΩ cm was used in all experiments.

Preparation of PVA hydrogel.

1.0 g PVA and 10 mL water were mixed and heated to 90 °C under stirring until the solution became clear, and then 83 μL hydrochloric acid solution was added to the cooled blended solution. Next, 1.0 g diluted of the aqueous GA solution (2%) was added to the blended solution under stirring to react for 10 s, and then the mixture was quickly poured into a Petri dish (diameter = 90 mm) and stored for 1 h. The PVA hydrogel (thickness: ca. 2 mm) was soaked into 200 mL water for 12 h and three times to remove hydrochloric acid. Finally, the obtained PVA hydrogel was stored in water.

Preparation of *κ*-CG hydrogel (hydrogel bonded with ionic groups).

0.2 g *κ*-Carrageenan was added to 10 mL water and stirred under 80 ^{o}C until the solute dissolves absolutely. After cooling, 1.0 g acetic acid and 1.0g aqueous GA solution (2%) were added to the solution. The *κ*-Carrageenan hydrogel was obtained after the mixture was poured into the model for 3 days.

Preparation of the dual ionic hydrogel (DIH) and ions-infused hydrogels.

The as-prepared PVA and κ-CG hydrogels were soaked into the 100 mL $CaCl_2$ solution (0 ~ 30 wt%) and NaCl solution (20 wt%) for 24 h and 3 times, respectively. Then the NaCl-infused PVA hydrogel, NaCl-infused κ-CG hydrogel, $CaCl_2$-infused PVA hydrogel and $CaCl_2$-infused κ-CG hydrogel (the DIH) were obtained. As the hydrogels were prone to shrink during the storage process, all the samples were stored in the soaked solutions for at least 5 days for further characterization.

Characterization of samples.

Scanning electron microscopy (SEM) observations were carried out on a Verios G4 UC field emission scanning electron microscope (Thermo scientific) operated at 2 kV. The samples were freeze-dried and then coated with a layer of Pt by ion sputtering before SEM observations. Raman spectra were measured using a Renishaw InVia Reflex Raman spectrometer operated by the laser at 532 nm as the

excitation source with 1% power (100mW). The surfaces, focused by a 50× objective lens (NA = 0.4), were scanned in the spectral region from 2800 cm^{-1} to 4000 cm^{-1} by accumulating over 3 scans and 10 s exposure time, giving a spectral resolution < 1 cm^{-1}. Appropriate corrections were made to obtain a flat baseline. The melting and crystallization points of hydrogels were obtained by Differential Scanning Calorimeter (DSC, Q2000, TA instruments) from a minimum -70˚C to 20˚C. A cooling/heating rate of 3˚C/min was used under the nitrogen atmosphere and at a flow rate of 40 mL/min. Thermal analysis consisting of thermogravimetric (TG) and differential thermal analysis (DTA) was performed to evaluate their thermal behavior on the PerkinElmer instrument (Diamond TG/DTA). Water contact angle tests were carried out on the OCA20 instrument (Dataphysics) with a droplet volume of 4 μL. The stress-strain curves of samples were obtained under the tension mold with a speed of 2 mm/s on an MTS instrument. The transmittance of the samples during the anti-frost test was roughly estimated on the basis of the grayscale of the stage under the samples, in which the initial grayscale is normalized as the 100% relative transmittance. In detail, a black dot was marked on the stage and then the photos of samples with time were recorded. After that, the grayscale of the black dot on the photos was measured by the software.

Lifespan assessment of hydrogel

The lifespan is defined by the period in which a hydrogel becomes structurally rigid or dry at ca. room temperature. Firstly, the hydrogel was placed in an environment with constant temperature (20 ^{o}C) and RH (50%). Then the flexibility and softness of the hydrogel were observed. When either of the functions fails, the stored time was considered as the life span of the hydrogel. It should be noted that the lifespans of some references without the dry/rigid information were estimated by the weight loss ratio of the samples. During the long-term lifespan assessment of DIH, the samples were stored in the room environment (temperature: ca.15-35 ^{o}C; relative humidity: ca. 30-90%).

Self-replenishment of Water for DIH

The self-replenishment of the water includes the weight measurement of the samples under periodically alternative RHs and after freezing dry, respectively. During the periodically alternative RHs test, the sample was firstly weighed, and then deposited in the environment with a RH of 70% for 12 h and the weight was recorded. Next, the sample was deposited into the chamber with a RH of 30% for 12 h and the weight was recorded as well. The periodically alternative cycles repeated 5 times in this work. The self-replenishment of the samples after freeze-drying was carried out by weighing the

as-freeze-dried samples with time at room temperature under a RH of ca. 50%. The hydrogels were freeze-dried and then the weight of samples was recorded with time.

Droplet freezing time test.

The prevention of droplet freezing was characterized by the droplet freezing time on surfaces via the contact angle measuring instrument (OCA20, Dataphysics). The instrument was equipped with a cooling stage (TP104SG, Instec Inc). A side-view camera was used to capture the performance of the droplets. The samples were deposited on the flat plate and then cooled to -10 ^{o}C for at least 5 min to get a stable target temperature. The water droplets (4 μL) were then deposited on the sample surfaces and the icing process of the droplets was recorded by the camera. The droplet freezing time is defined as the interval between the time when water droplet is deposited on the surface and the time when ice forms. During the tests, the environmental temperature was ca. 20 ^{o}C and the relative humidity was ca. 50%.

Anti-frost test.

The dry N_2 was used to keep the surface without frost before the anti-frost test. The anti-frost tests of samples were characterized by observing the frost formation on sample surfaces, in which the cooling stage (TP104SG, Instec Inc) was used to regulate the temperature. A room humidity controller was used to regulate the RH. Before the test, the environmental RH was recorded as 50% at ca. 20 ^{o}C after operation of the room humidity controller. The samples were then mounted on the flat cooling plate, and cooled to the target temperature (-10 ^{o}C) for 5 min, when the dry N_2 was used to blow on the surface to avoid frost formation before recording the process. The surface of the sample starts to be observed when the dry N_2 was removed, and the anti-frost time starts to record. The frost formation time at the target temperature and humidity is defined as the interval between the time when the dry N_2 is removed from the surfaces and the time when ice appears.

Ice adhesion strength test.

Ice adhesion strength was measured by a force transducer (ZTS-500) equipped with a motorized linear stage (Zaber's X-LRQ-DEC), and a cooling stage (TP104SG, Instec Inc). The schematic of the setup is shown in Figure 4c of the main manuscript. A cylinder with a 1 mm thick wall and 15 mm inner diameter was placed onto the sample surfaces acting as an ice mold, and then 2.5 g deionized water was used for formation of ice. Before the ice adhesion test, water was filled in the cylinder on the surface of samples and allowed to form ice at ca. -50 ℃, in which the PMMA lid (box without base) is covered on the setup to mitigate the heat transfer. Then the samples with the ice cylinder were kept at

the temperature (-10 ℃) for at least 5 min to reach equilibrium for further adhesion test. During the ice adhesion test, a force probe with a 4 mm diameter propelled the tube-encased ice columns under a velocity of 0.075 mm s^{-1}, with the probe aligned close to the tested surface (less than 2 mm) to minimize the torque on the ice cylinder. The loading curves were recorded, and the peak value of the shear force was divided by the ice contact area on the surface to obtain the ice adhesion strength.

Molecular dynamics (MD) simulations

Linear *k*-CG polymer chains with and without -SO_3^- groups were placed in a rectangular box with dimensions of 40×100×120 $Å^3$. Three different solutions of pure water, NaCl and $CaCl_2$ were added into the box. To mimic the systems, the CVFF force-field[1] was used with mathematical expression as follows

$$E_{\text{pot}} = \overbrace{\sum_{b} D_b(b-b_0)^2}^{(1)} + \overbrace{\sum_{\theta} H_\theta(\theta-\theta_0)^2}^{(2)} + \overbrace{\sum_{\phi} H_\phi[1+s cos(n\phi)]}^{(3)} + \overbrace{\sum_{\chi} H_\chi \chi^2}^{(4)}$$
$$+ \overbrace{\sum_{b}\sum_{b'} F_{bb'}(b-b_0)(b'-b'_0)}^{(5)} + \overbrace{\sum_{\theta}\sum_{\theta'} F_{\theta\theta'}(\theta-\theta_0)(\theta'-\theta'_0)}^{(6)}$$
$$+ \overbrace{\sum_{b}\sum_{\theta} F_{b\theta}(b-b_0)(\theta-\theta_0)}^{(7)} + \overbrace{\sum_{\phi} F_{\phi\theta\theta'}cos\phi(\theta-\theta_0)(\theta'-\theta'_0)}^{(8)} + \overbrace{\sum_{\chi}\sum_{\chi'} F_{\chi\chi'}\chi\chi'}^{(9)}$$
$$+ \overbrace{\sum \epsilon[(r*/r)^{12} - 2(r*/r)^6]}^{(10)} + \overbrace{\sum q_i q_j/\epsilon r_{ij}}^{(11)}$$

where E_{pot} is the total potential energy derived from the CVFF forcefield. Terms (1)-(4) are harmonic contributions of stretching and compression of covalent bonds (b), angle bending (θ), internal rotation or torsion of dihedral angle (φ), and out-of-plane improper angles (χ), respectively. Terms (5)-(9) are related to cross-interactions, for example, term (7) is related to the stretch-bend cross-interaction.

Due to the high initial potential energy of the cells, cell relaxation becomes necessary before carrying out further calculations. In addition, the constructed initial amorphous cells contained regions with very different density values. For these reasons, cells were firstly relaxed using MD simulations to achieve more homogeneous distributions of atoms, with lower energy contents. In order to do that, cells were exported to the Large-scale Atomic/Molecular Massively Parallel Simulator (LAMMPS)[2]. LAMMPS input data file contains information related to the molecular topology and force-field parameters (CVFF)[1].

Initially, as-constructed samples were started with energy minimization by the Polak-Ribiere version of the CG algorithm[3-4]. Afterward, MD relaxation with simulation time of 0.5 ns was performed under NPT (constant number of particle, pressure, and temperature) ensemble at pressure of 1 atm and temperature of 300 K to realize a stable sample. Finally, MD simulations under NVT ensemble were performed at 300 K for 2 ns to compute the mean square displacements (MSD) of ions and water, as well as their density distributions. Both pressure and temperature were controlled by Nosé-Hoover technique[3-4]. A time step of 1 fs was adopted. A cut-off value of 12.0 Å was used for Lennard-Jones potential. Long-range electrostatic terms were calculated with an efficient particle-particle particle-mesh (PPPM) solver.[5]

The ensemble-averaged MSD is defined as:

$$\mathrm{MSD}(t) = \frac{1}{N}\langle \sum_{j=1}^{N} \left[\vec{R}_j(t) - \vec{R}_j(0)\right]^2 \rangle$$

where $\vec{R}_j(0)$ and $\vec{R}_j(t)$ are the position vectors of the same particles (index *j*) at some initial *t*=0 and at some later time (*t*), respectively, *N* is the total number of particles, and $\langle \cdots \rangle$ denotes the ensemble average. The isotropic nature of MSD is evident. The diffusion coefficient can be extracted from the long-time MSD using $\langle (\Delta r)^2 \rangle = 2nD\Delta t$, where *n* stands for dimensions involved in the system and *D*: the diffusion coefficient.

References:

(1) Dauber-Osguthorpe, P.; Roberts, V. A.; Osguthorpe, D. J.; Wolff, J.; Genest, M.; Hagler, A. T. Structure and energetics of ligand binding to proteins: Escherichia coli dihydrofolate reductase-trimethoprim, a drug-receptor system. *Proteins: Structure, Function, and Bioinformatics* **1988,** *4* (1), 31-47, DOI: 10.1002/prot.340040106.

(2) Plimpton, S. Fast Parallel Algorithms for Short-Range Molecular Dynamics. *Journal of Computational Physics* **1995,** *117* (1), 1-19, DOI: 10.1006/jcph.1995.1039.

(3) Nocedal, J.; Wright, S. *Numerical optimization*, Springer Science & Business Media: 2006.

(4) Gilbert, J. C.; Nocedal, J. J. S. J. o. o. Global convergence properties of conjugate gradient methods for optimization. **1992,** *2* (1), 21-42.

(5) Lock, N.; Wu, Y.; Christensen, M.; Cameron, L. J.; Peterson, V. K.; Bridgeman, A. J.; Kepert, C. J.; Iversen, B. B. Elucidating Negative Thermal Expansion in MOF-5. *The Journal of Physical Chemistry C* **2010,** *114* (39), 16181-16186, DOI: 10.1021/jp103212z.

Figures and Table:

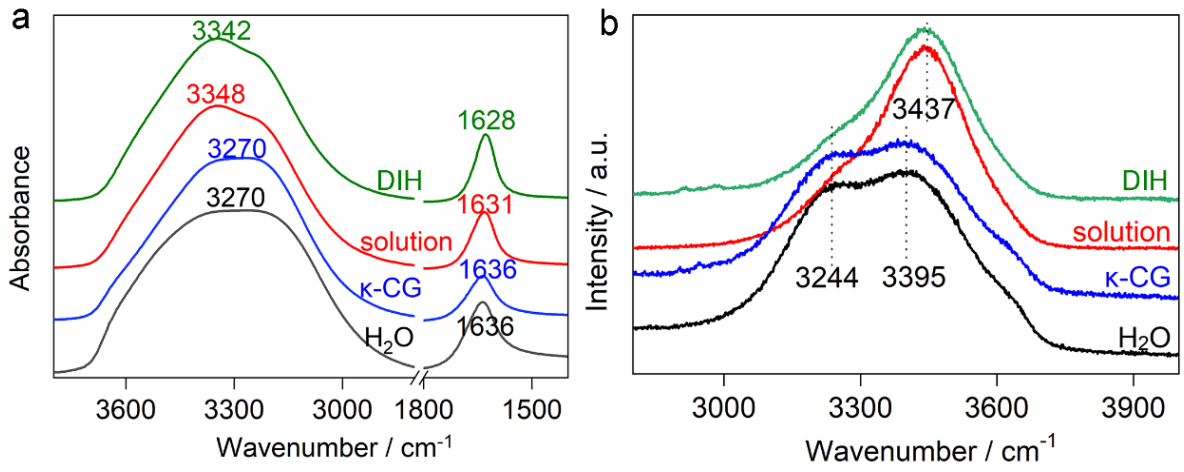

Figure S1 (a) IR and (b) Raman spectra of DIH in comparison with water, κ-CG hydrogel and 30 wt% $CaCl_2$ solution.

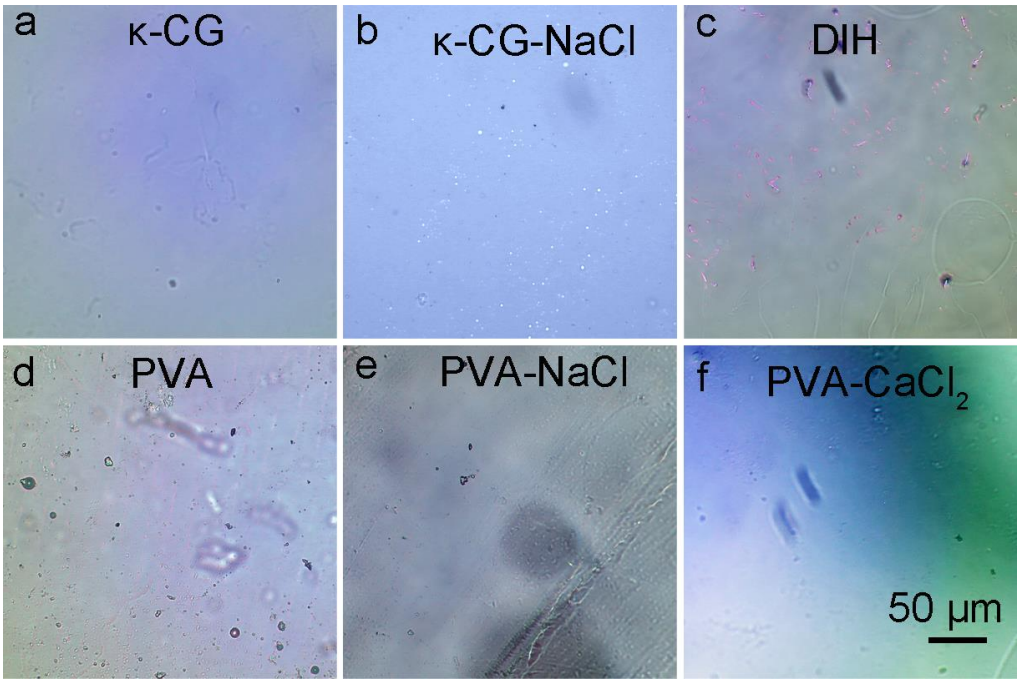

Figure S2 Microphotographs of hydrogels. The κ-CG, κ-CG-NaCl hydrogels and DIH have sufficient liquid on their surfaces, while the PVA and PVA-NaCl hydrogels are covered with small isolated droplets.

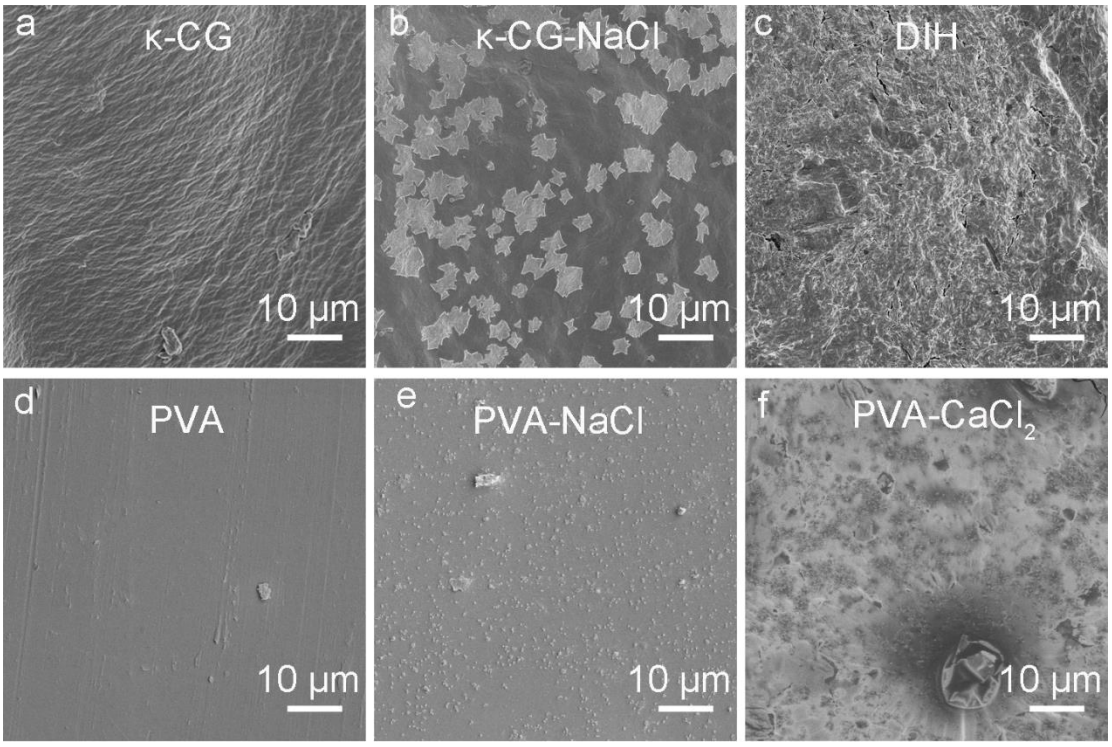

Figure S3 Top-view SEM images of hydrogels after lyophilization. In contrast to the pristine κ-CG and PVA hydrogels with nothing on their surfaces, the surfaces of free ions-infused hydrogels are all covered by salt. In detail, salts aggregates on the surfaces of NaCl-infused hydrogels after lyophilization. The $CaCl_2$ are dispersed on the surfaces of PVA-$CaCl_2$ hydrogel. In contrast, $CaCl_2$ does not separate obviously from the DIH surface, indicating it has strong action with $CaCl_2$.

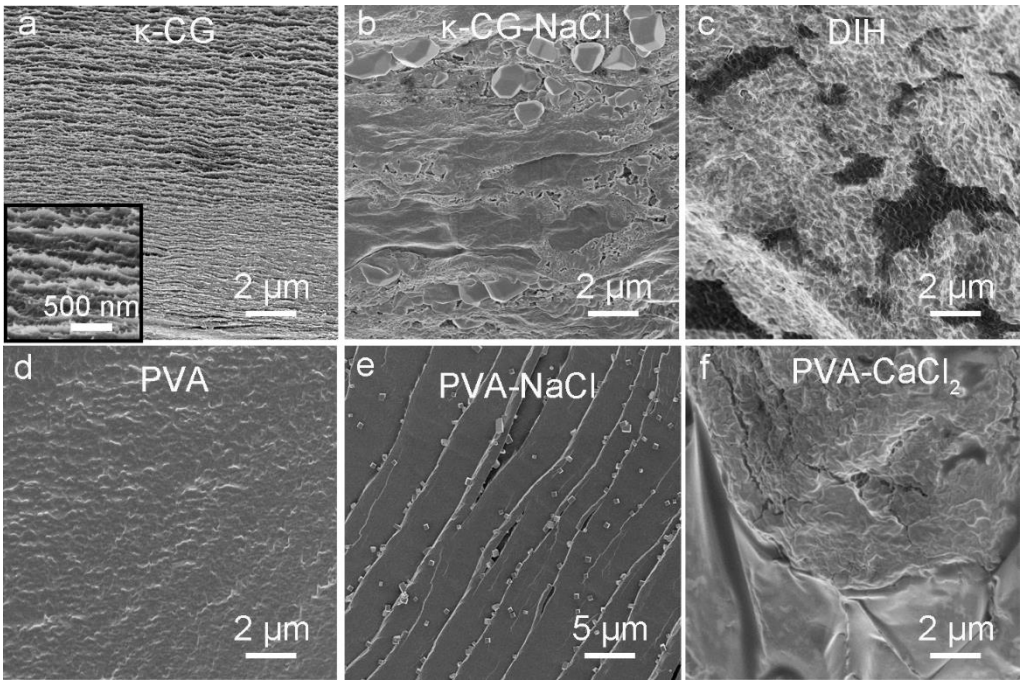

Figure S4 Cross-sectional SEM images of hydrogels after lyophilization. The PVA and κ-CG have a nanoporous structure. NaCl crystalline particles separate and are dispersed inside the PVA-NaCl and κ-CG-NaCl hydrogel structures. The cross-sectional images of DIH show the homogeneously dispersed white/gray pattern, indicating the $CaCl_2$ are homogeneously dispersed inner the DIH structure. The $CaCl_2$ seems to aggregate inside the PVA-$CaCl_2$ hydrogel.

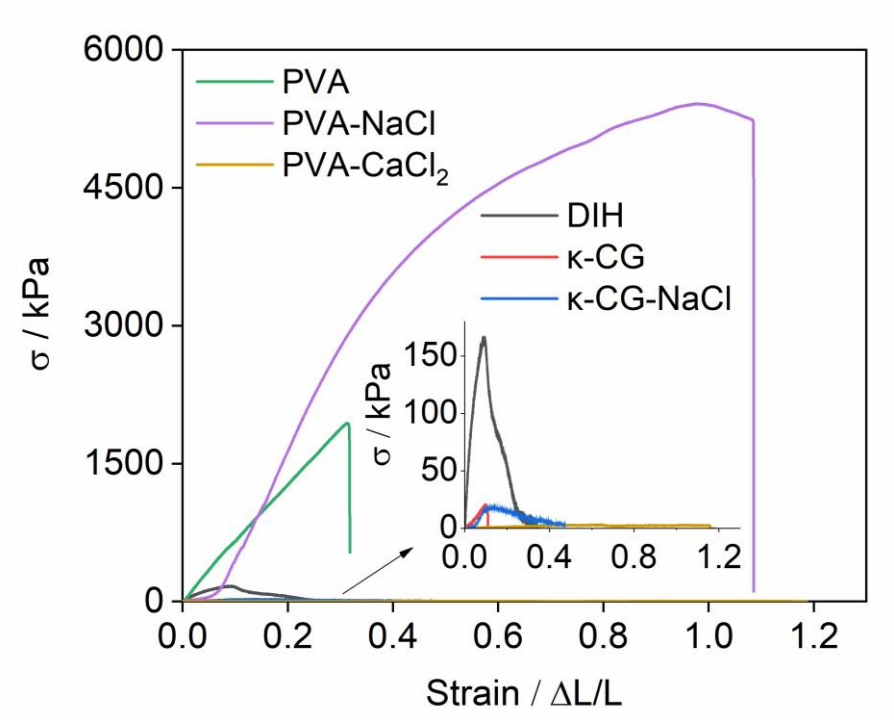

Figure S5 Strain-stress curves of various hydrogels. It should be noted that the samples are investigated after storage, in which the water content of all the hydrogels keep at a stable state.

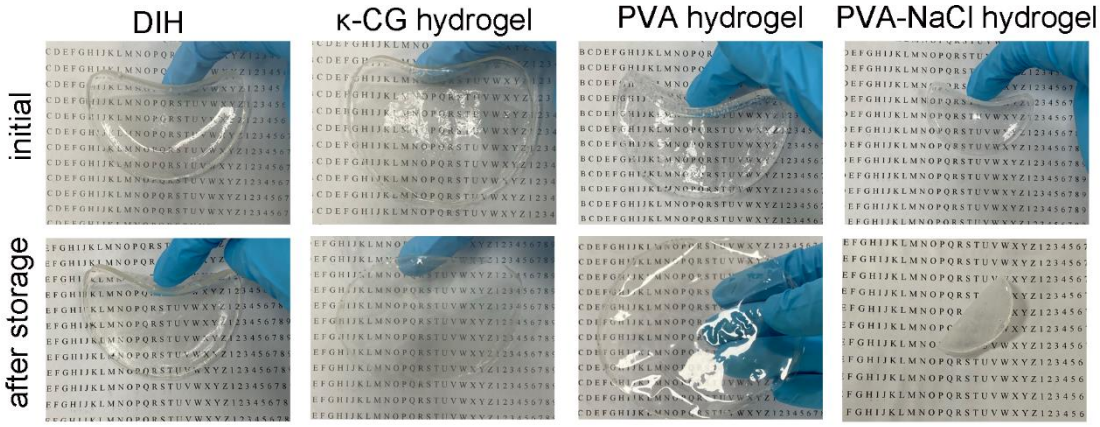

Figure S6 Digital images of DIH before and after storage for 24 h in comparison with κ-CG hydrogel, PVA hydrogel and 20 wt% NaCl solution infused PVA hydrogel.

Table S1 Lifespan of various hydrogels.

Types of hydrogels	Name of samples	Relative humidity (RH) / %	Temperature / °C	Time / h	References
dual-ionic hydrogels	k-CG-$CaCl_2$	50	RT	5760	This work
	k-CG-NaCl hydrogel	50	RT	6	This work
hydrogels (without ions)	PVA hydrogel	50	RT	9	This work
	PAAm-alginate hydrogel	50	RT	24	Nat. Commun., 2016, 7, 12028.
	water-based Al-NC-G gel	50	RT	36	ACS Appl. Mater. Interfaces., 2021, 13, 21822-21830.
	water-based Ca-alginate/PAAm hydrogel	50	RT	24	Angew Chem Int Ed Engl., 2018; 57:6568-6571.
organohydrogels	glycerol hydrogel	50	RT	360	Angew Chem Int Ed Engl., 2018; 57:6568-6571.
	NC-G-80 gel	60	27	240	Polymers (Basel), 2018, 10,1025
	Al-NC-G gel with glycerol (1:1)	50	RT	720	ACS Appl. Mater. Interfaces., 2021, 13, 21822-21830.
	Al-NC-G gel with glycerol (2:1)	50	RT	720	ACS Appl. Mater. Interfaces., 2021, 13, 21822-21830.
elastomer-hydrogels hybrid	hydrogel–Ecoflex hybrid	50	RT	48	Nat. Commun., 2016, 7, 12028.
	hydrogel–elastomer	50	26	624	ACS Appl. Mater. Interfaces.,2017, 9, 30, 25542–25552
	H-TENG	40	20	672	ACS Appl. Mater. Interfaces, 2020, 12, 23474–23483
hydrogel bonded with ionic groups	k-CG hydrogel	50	RT	12	This work
free ions-infused hydrogels	EG-NaAc hybrid hydrogel	60	25	28	Colloids Surf., A., 2020, 607, 125443.
	PVA-NaCl hydrogel	50	RT	6	This work
	PVA-$CaCl_2$ hydrogel	50	RT	*	This work

RT: room temperature. *The life span of PVA-$CaCl_2$ is not suitable to estimate based on the criterion.

Figure S7 The evolution of as-freeze-dried DIH with time.

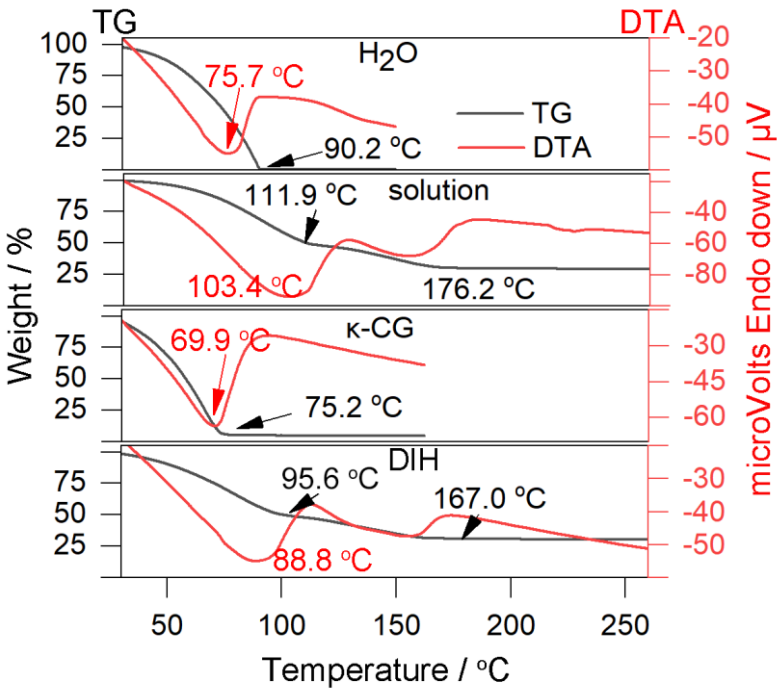

Figure S8 TG-DTA curves of DIH in comparison with water, κ-CG hydrogel and 30 wt% $CaCl_2$ solution.

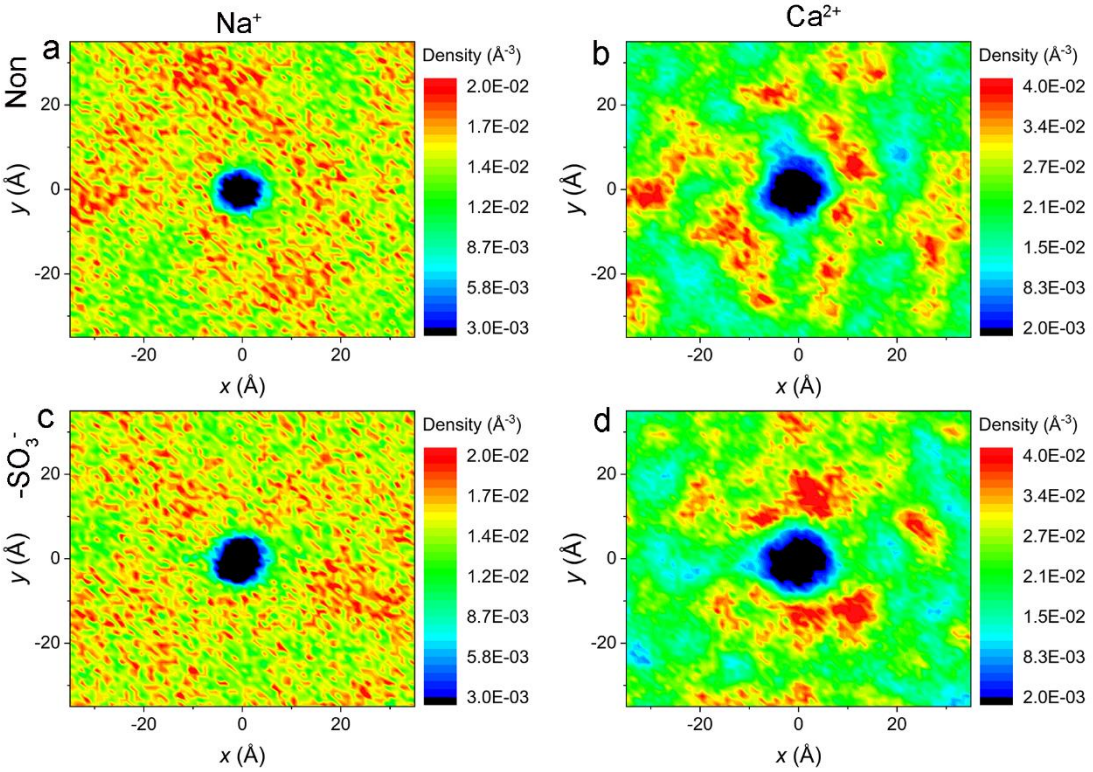

Figure S9 (a-d) Density distribution of Na^+ and Ca^{2+} in hydrogels with and without $-SO_3^-$. In a-d, the black area in the center of density distribution represents the approximate range of DIH motion. Compared with Na^+ solution, Ca^{2+} is easier to aggregate.

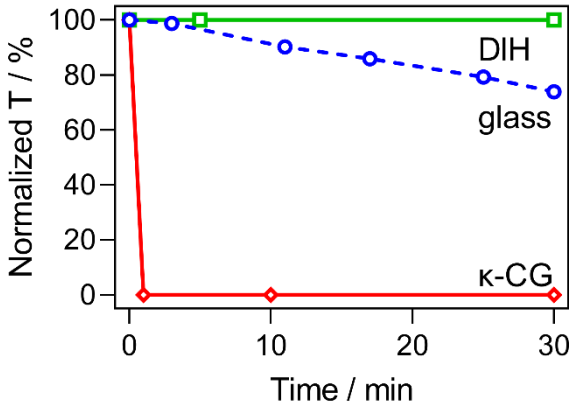

Figure S 10 Normalized transmittance of glass, κ-CG and DIH with time under -10 °C and RH of 50%. The transmittance under low temperature was estimated by the greyscale of the stage with a black dot.

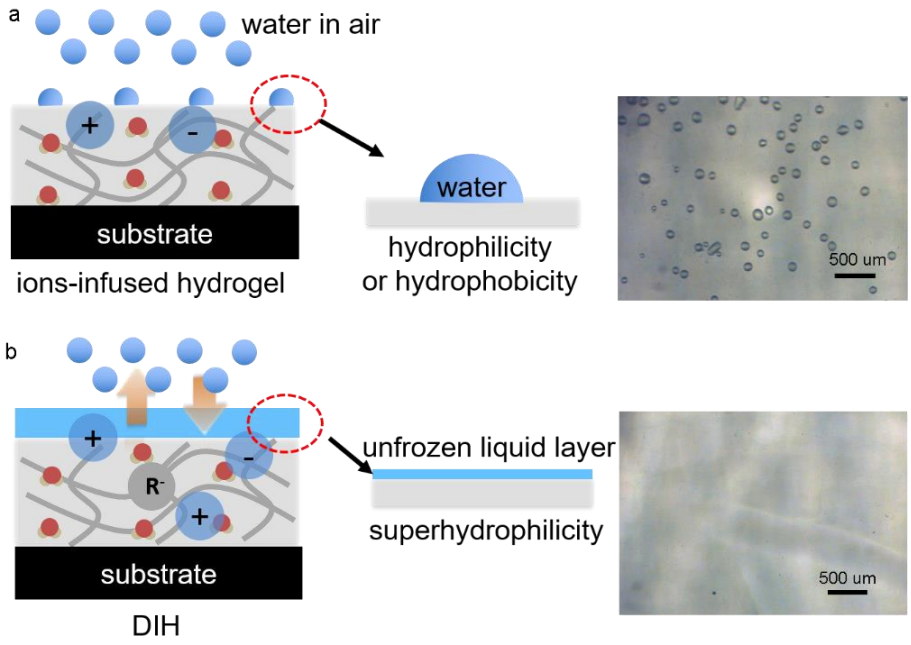

Figure S11 Schematics and micrographs of (a) 20 wt% NaCl-infused hydrogel and (b) DIH surface under a RH of 50% and -10 ^{o}C after 30 min. The droplets appear on the 20 wt% NaCl-infused surface, indicating fog formation on the surfaces.

CRediT authorship contribution statement

Tong Li: Conceptualization, Data curation, Funding acquisition, Investigation; Methodology, Project administration, Writing – original draft, Writing – review & editing. Ke Xu: Data curation, Methodology. Lianxin Shi: Methodology, Writing – review & editing. Jianyang Wu: Data curation, Writing – review & editing, Funding acquisition. Jianying He: Supervision, Writing –review & editing , Funding acquisition. Zhiliang Zhang: Supervision, Writing – review & editing, Funding acquisition.